Table 1. Results obtained for the four optimization and two static discretization methods

	Number of rules	Computation time (s)	AUC
Genetic algorithm	172	3726	0.6748
Particle swarm	146	1690	0.6718
Hill climbing	209	12624	0.6902
Simulated annealing	197	1159	0.6802
Equal width bin	231	2	0.5952
Equal frequency bin	307	2	0.5986

rejections of 200 and a maximum number of successes within one temperature set to t_0.

Table 1 shows that, albeit marginal, HC produces the highest classification accuracy when using the AUC measure. SA optimization has the lowest computational time with respect to the optimized methods. From Table 1, it is evident that the computational time required for the static EWB and EFB partitioning is much less than that for the optimized approaches. Having said that, the higher forecasting accuracy obtained using optimized methods results in more concrete evidence from which policies can be generated. Fewer rules are also generated from the optimized methods approach, and it is from these extracted rules that the causal interpretations are then formulated by a linguistic approximation.

The results indicate that the proposed method of using optimization techniques to granulize/discretize rough set partitions is feasible and it also produces higher forecasting/classification accuracies than the EWB and EFB partitioning. Among the four optimization techniques, it can be stated that no particular technique is superior to another. There are marginal differences in the accuracies produced (using AUC), but in all cases easy-to-interpret, linguistic rules are generated.

The results of both datasets indicate that the optimized methods produce higher forecasting/classification accuracies than the static EWB and EFB partitioning methods. When comparing the optimized approaches against each other, as expected there is no significant difference between the methods used. The rough sets produce a balance between transparency of the rough set model and accuracy of HIV estimation, but it does come at a cost of high computational effort.

1. Pawlak, Z., *Rough Sets, Theoretical Aspects of Reasoning about Data*, Kluwer Academic Publishers, 1991, p. 33.
2. Garson, G. D., *Soc. Sci. Comput. Rev.*, 1991, **9**, 399–433.
3. Komorowski, J., Pawlak, Z., Polkowski, L. and Skowron, A., *The Handbook of Data Mining and Knowledge Discovery*, Oxford University Press, 1999.
4. Grzymala-Busse, J. W., In Proceedings of the Rough Sets and Emerging Intelligent Systems Paradigms, June, 2007, pp. 12–21.
5. Jaafar, A. F. B., Jais, J., Hamid, M. H. B. H. A., Rahman, Z. B. A. and Benaouda, D., In Proceedings of the 4th International Conference on Multimedia and Information and Communication Technologies in Education, Seville, Spain, November 2006.
6. Marwala, T., *Computational Intelligence for Modelling Complex Systems*, Research India Publications, Delhi, 2007.
7. Crossingham, B. and Marwala, T., In *Studies in Computational Intelligence*, Springer-Verlag, 2007, vol. 78, pp. 245–250.
8. Lasry, A., Zaric, G. S. and Carter, M. W., *Eur. J. Oper. Res.*, 2007, **180**, 786–799.

Received 31 March 2008; revised accepted 24 September 2008

TSHILIDZI MARWALA*
BODIE CROSSINGHAM

School of Electrical and Information Engineering,
University of the Witwatersrand,
Private Bag X3, WITS,
2050, South Africa
**For correspondence.*
e-mail: tshilidzi.marwala@wits.ac.za

Occurrence of zincian ilmenite from Srikurmam placer sand deposit, Andhra Pradesh, India

Placer deposits of Andhra Pradesh (AP) particularly ilmenite occur at Bhavanapadu, Kalingapatnam, Srikurmam and Donkuru-Barua in Sikakulam District, Bhimunipatnam in Visakhapatnam–Vizianagaram districts, Kakinada in East Godavari District and Nizamapatnam in Guntur and Prakasham districts. Srikurmam mineral sand deposit is one of the largest placer deposits established from this region (A. Y. Rao *et al.*, unpublished). The deposit is confined between two prominent lineament-controlled rivers, Nagavali and Vamsadhara, and spans over a coastal length of 22 km. Geomorphic units are dominated by the presence of structurally controlled estuarine rivers, viz. Nagavali in the south and Vamsadhara in the north. A tidal creek and a geomorphic-low, lppligedda, occur to the north-central part of the area (Figure 1). The fore dune and rear dune are well developed, whereas inter dune is masked at places. The dunes generally rise to a height of 18 m in the rear, as a consequence of resting on higher basement of palaeo-dunal-beach complex (Figure 2). It is a general assumption that the source of heavy minerals for the deposit is the granulite facies rocks of Khondalite group. Charnockite has a restricted occurrence in the hinterland, dominated by Khondalite. Upper Gondwana formations occur to the south-west of the deposit. The area also receives its detrital material from the older reddened dunes exposed along the western margins and the offshore bars. Preliminary investigations have revealed a total mineral content of 30 million tonnes at a working grade of 34.36%, and is by far the richest deposit in this part of the coast. Marginally higher garnet content (37.10%) has been estimated along with an ilmenite content of 31.94% (A. Y. Rao *et al.*, unpublished). Ramana (unpub-

lished) studied the geochemistry and ore mineralogy of ilmenites from this area. He indicated that these ilmenites are rich in certain trace elements, such as V, Zn, Ce, Nb, Cr. Similarly, the ore mineralogy also indicated a high degree of variability.

Samples were collected from both beach and dunal complex. The sampling methodology and laboratory techniques for heavy-mineral quantification adopted in this study are according to the earlier investigations[1] (J. V. Ramana, unpublished). The samples were washed thoroughly, de-silted and oven-dried, and studied under binocular microscope to find the overall heavy mineral concentration and heavy mineral suite. Four samples were selected for the detailed investigations, and were subjected to sieve analysis for 15 min in ASTM sieves set at $1/2\phi$ interval on a Ro Tap-type sieve shaker. The fractions obtained from the sieve analysis were subjected to magnetic separation using a bar magnet and the non-magnetic fractions were further subjected to heavy liquid separation (bromoform, specific gravity 2.89 g/cm^3), following standard procedure. Heavies obtained from the heavy liquid separation of the fractions were further subjected to isodynamic separation at 0.275 Å for separation of ilmenite. The purity of the ilmenite separated was ensured to be more than 99%, by examining the fractions under binocular microscope.

Microscopic observations revealed that magnetic heavy mineral fractions were dominated by ilmenite. Ilmenites are of two types. One type has rounded-off corners, is grey-white coloured, with high relief and varying reflectivity. The poorly reflected parts of the grains could be due to minor alteration. The other type is relatively fresh, angular to sub-angular and grey in colour. Its associated magnetite is also of the same size and shape, but exhibits alteration along the periphery.

Some of the ilmenite grains, though few in number (2–5 grains per 100 grains), show conspicuous optical characteristics like tabular form, dark brown to black colour and different reflectance characteristics compared to other ilmenite grains. These grains were noticed in samples from both beach and dune environments. These are attractive, which prompted us to undertake the EPMA study (Figure 3). These grains were separated carefully by hand-picking, and seven grains (S1–S7) were subjected to EPMA studies. The results (Table 1) indicate that these ilmenite grains have a characteristic feature of high zinc concentration, which varies from 2.09 to 2.66%. When these ilmenites were compared with the earlier report of zincian ilmenite[2], compositionally there was an exact match (Table 2). The XRD studies of these grains further confirmed them to be of zincian ilmenite, which is part of the zincian ilmenite-Ecandrewsite solid solution (Table 3)[3].

Based on the above observations the occurrence of zinc-bearing ilmenite or

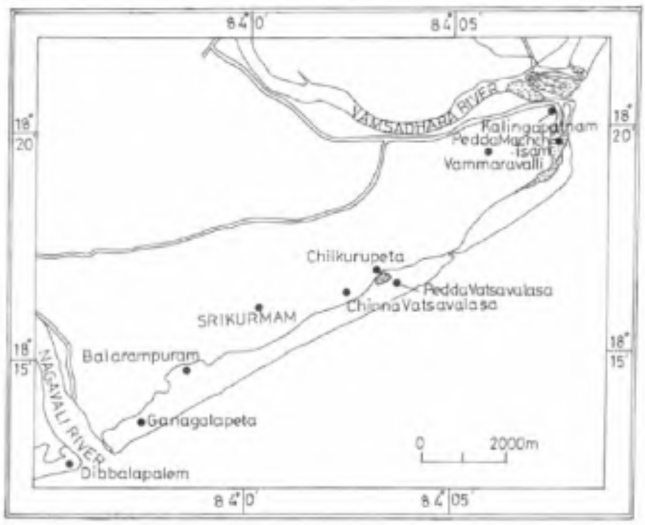

Figure 1. Srikurmam mineral sand deposits, Srikakulam.

Figure 2. Density stratification in the berm cut, Srikurmam deposits.

Table 1. EPMA data of zincian ilmenite in the present study

Oxide	S1	S2	S3	S4	S5	S6	S7
TiO_2	50.91	50.8	32.49	53.06	52.1	51.01	52.76
FeO	45.5	45.62	61.32	43.1	42.29	44.16	42.89
Al_2O_3	0.02	0.01	0.01	0.01	0.01	0.01	0.02
MnO	1.13	1.15	0.01	0.5	0.49	1.15	0.50
MgO	0.4	0.41	0.49	2.09	2.12	0.40	2.11
ZnO	2.09	2.12	2.66	2.25	2.26	2.14	2.39
Total	100.05	100.11	96.98	101.01	99.27	98.87	100.67

Figure 3. Zincian ilmenite in the ilmenite population under binocular microscope, 50×.

Table 2. Representative composition of zincian ilmenite[2]

Oxide	1	2	3	4	5	6	7
TiO_2	53.23	52.56	52.36	52.43	52.57	52.49	52.77
FeO	43.04	45.78	40.07	41.73	46.23	46.71	46.07
Al_2O_3	0.01	0.11	0.02	0.00	0.00	0.00	0.00
MnO	0.92	0.61	0.59	0.61	0.68	0.61	0.57
MgO	0.07	0.08	0.19	0.19	0.15	0.17	0.14
ZnO	2.81	1.00	6.47	5.43	0.26	0.10	0.58
Total	100.08	100.14	99.70	100.39	99.89	100.08	100.13

Table 3. XRD data of ilmenites in the present study indicating similarity with standard zincian ilmenite-Ecandrewsite peaks[3]

	S_1	S_5
E d-spacing (Å)	*d*-spacing (Å)	*d*-spacing(Å)
2.73	2.722	2.722
2.53	2.522	2.522
1.71	1.71	1.71
2.23	2.217	2.217
1.87	1.856	1.856
3.69	3.68	3.683
1.502	1.49	1.49

zincian ilmenite along this coast can be clearly established.

Ecandrewsite is a zinc analogue of ilmenite, which was first described from broken Hill[3]. A number of researchers later explained the paragenesis of zincian ilmenite. Plimer[4] argued, from field and textural evidence, that zincian ilmenite-Ecandrewsite is formed by the reaction of rutile, anatase or ilmenite with zincian clays or carbonates during prograde metamorphism. Alternatively, (Zn, Fe) TiO_3 may form from desulphidation of sphalerite or by breakdown of zinc-bearing minerals such as staurolite, biotite or hogbomite, similar to what has been proposed for the formation of zincian spinel[5–7]. Zincian ilmenite also occurs in granite in Fuzhou, China[8], which indicates that it may also precipitate directly form hydrothermal solutions.

Zincian ilmenite-Ecandrewsite was reported from a pelitic schist, Death Valley, California[2]. According to the investigators, the paragenesis of zinc-bearing ilmenite solid solution in metapelitic rocks is problematic. Thermodynamic calculations and comparison with other reported occurrences indicate that ilmenite with greater than a few mol% $ZnTiO_3$ component in metapelitic rocks should be metastable relative to gahanite + quartz + rutile, over the range of geologically relevant conditions of regional metamorphism. Based on the thermodynamic calculation, they have concluded that the metastable phases are not generally believed to persist during an extended period of regional metamorphism. Hence they confirmed that ilmenite, containing more than a few mol% $ZnTiO_3$ in this area and in other regionally metamorphosed metasedimentary rocks, formed during short-lived metasomatic events that post-dated the peak of regional metamorphism. At the Death Valley, this interpretation is supported by the presence of late-stage dykes of granitic pegmatite that crosscuts the pelitic schists and may have provided fluid for the metasomatic event.

Similar environments were also reported in the Eastern Ghats mobile belt. Grew *et al.*[9] have reported a characteristic mineralogical assemblage from quartz–sillimanite–hypersthene–cordierite gneisses from Venugopalapuram, Vizianagaram District, AP. The assemblage consists of spinels, including hemo ilmenite, magnetite and zincian hogbomite. This explains the fact that there exists similar environments and events which are of post-granulitic metamorphism.

Ramana (unpublished) indicated that the ilmenites from Srikurmam deposit might have been derived from more than two sources based on the ore mineralogical and geochemical variability. This report on the occurrence of zincian ilmenite in a placer deposit may be the first of its kind in India. This strongly supports the idea of diverse compositional ilmenites, the source of which cannot and need not be attributed to only the Eastern Ghats hinterland, The paragenesis of zincian ilmenite established elsewhere indicates that it may form in the regionally metamorphosed metasedimentary rocks, during short-lived metasomatic events that post-date the peak of regional metamorphism. The recent reports[9] on the existence of such environments in the Eastern Ghats, may indicate that zincian ilmenite is probably a derivative of such a metasomatic event of post-granulitic phase.

1. Jagannadha Rao, M., Venkata Ramana, J., Venugopal, R. and Chandra Rao, M., *J. Geol. Soc. India*, 2006, **66**, 147–149.
2. Whitney, D. L., Hirschmann, M. and Miller, M. G., *Can. Miner.*, 1993, **31**, 425–436.
3. Birch, W. D., Burke, E. A. J., Wall, V. J. and Etheridge, M. A., *Miner. Mag.*, 1988, **52**, 237–240.
4. Plimer, I. R., *Neues Jahrb. Miner., Monatsh.*, 1990, **30**, 529–536.
5. Stoddard, E. F., *Am. Miner.*, 1979, **64**, 736–741.
6. Dietvorst, E. J. L., *Contrib. Mineral. Petrol.*, 1980, **75**, 327–337.
7. Spry, P. G. and Scott, S. D., *Econ. Geol.*, 1986, **81**, 1446–1463.
8. Suwa, K., Enami, M., Hiraiwa, I. and Yang, T., *Miner. Petrol.*, 1987, **36**, 111–120.
9. Grew, E. S. *et al.*, *Miner. Mag.*, 2003, **67**, 1081–1098.

ACKNOWLEDGEMENTS. We thank the Department of Science and Technology, New Delhi, for funds. We also thank Geological Survey of India, Hyderabad, for carrying out EPMA analyses of ilmenite samples.

Received 22 October 2007; revised accepted 24 September 2008

M. JAGANNADHA RAO[1,*]
AARON A. JAYA RAJ[2]
K. JOHN PAUL[2]

[1]*Department of Geology, Andhra University, Visakhapatnam 530 003, India*
[2]*Department of Geology, Acharya Nagarjuna University, Nagarjuna Nagar 522 510, India*
**For correspondence.*
e-mail: mjrao_isa@yahoo.co.in

A note on the recent earthquakes in the Bengal Basin

A mild tremor shook the Bengal Basin region when a shallow-depth earthquake[1,2] of m_b 4.3, M_L 4.0 with epicentre at 23.47°N, 87.12°E struck at 11 : 40 a.m. local time on 6 February 2008. Highest inflictions were observed in the epicentral zone of Bankura District, with the reported building damages in the surrounding areas. The event is significant because of its epicentral region being located in the seismic zone II of BIS: 2002 nomenclature[3] – the least seismic hazard classified, even though the inflicted damage distributions exhibited rather higher intensity. Approximately two years ago an earthquake of M_L 4.0 was also recorded at 3 : 10 p.m. local time on 13 December 2005, with its epicentre located at 22.31°N, 87.64°E. While, there is a perceptible vulnerability lest a bigger earthquake occurs, the recent earthquakes indicate a neo-tectonic activity along the underlying seismogenic source. Therefore, an insight into the related source attributes would be significant, given the implications of the perceived hazards in the region.

The tectonic framework of the region as depicted in Figure 1 *a* presents several prominent underlying faults in the region[4]. The Main Boundary Thrust, along with several other active faults, can be observed in the northern districts. To the west, the Garhmayna–Khanda–Ghosh fault stretching in the N–S direction connects to the Rajmahal fault in the north. Towards southwest, the Pingla fault is most predominant with a similar orientation. The December 2005 earthquake is apparently attributed to the Pingla fault. On the other hand, there is slight dislocation of the February 2008 earthquake to arrive at a similar conclusion. Nevertheless, given the proximity of these earthquakes in an otherwise passive region, it is likely that both events come under a single seismotectonic domain.

The two earthquakes were recorded by the Broadband Seismological Observatory at Indian Institute of Technology Kharagpur with GPS location of 22.31°N, 87.31°E. The observatory houses one ST-S2 broadband seismograph with free period of 120 s and electrodynamic constant of 1500 mV/mm/s, and a Q330 recorder with sensitivity of 419.430 counts/mV. Global Positioning System (GPS) synchronization has been provided to maintain the time in accordance with the Coordinated Universal Time (UTC), while the data sampling has been done at 100, 20 and 1 samples per sec respectively.

Figure 1 *b* depicts the recorded ground velocity (m/s) for both the earthquakes. The velocity data have been derived through deconvolution of the instrument response. Thereafter, the radial and transverse components have been computed by rotating the seismograms according to the corresponding back azimuths. Source parameterization in terms of corner frequency ω_c, seismic moment M_o, and stress drop $\Delta\delta$ has been estimated using *S*-phase displacement Fourier spectra of the recorded waveform data. Since the magnitude of the earthquakes is small, the standard Brune's ω^2-point source model for the average amplitude spectra for a circular dislocation in the frequency domain has been considered. The model is defined as:

$$A(\omega) = \mathrm{SO}(\omega, \omega_c)\mathrm{SI}(\omega)P(\omega)F(\omega, \omega_m), \quad (1)$$

where $\mathrm{SO}(\omega, \omega_c)$, $P(\omega)$, and $\mathrm{SI}(\omega)$ correspond to the source term, path term, and site function[5]. A high-cut filter $F(\omega, \omega_m)$ has been convolved with the model to stabilize the decay rate at higher frequencies. The path term is defined as:

$$P(\omega) = G(R)\mathrm{e}^{\frac{-\omega R}{2Q(\omega)\beta}}. \quad (2)$$

The path effect $G(R)$ is considered to be inversely proportional to the hypocentral distance R less than 100 km, and proportional[6] to $R^{-0.5}$ for R greater than 100 km. The path term referred to as the quality factor, has been taken to be constant in the present analysis, equivalent to 800 as proposed for the region[7].

The source term $\mathrm{SO}(\omega, \omega_c)$ is defined as:

$$\overline{\mathrm{SO}}(\omega,\omega_c) = \frac{[R_{\theta\phi}FS\omega^2]}{\sqrt{2}(4\pi\rho\beta^3)} * \frac{M_o}{1+(\omega/\omega_c)^\gamma}. \quad (3)$$

Following applicable standard convention[8], we assigned $\gamma = 2$, average radiation pattern $R_{\phi\varphi} = 0.6$, shear wave velocity $\beta = 3{\cdot}3$ km/s, free surface amplification FS = 2, and bedrock density $\rho = 2.7$ g/cm^3. A singular value decomposition algo-